Defect Passivation and Electron Band Energy Regulation of ZnO Electron Transport Layer through a Synergetic Bifunctional Surface Engineering for Efficient Quantum Dot Light-Emitting Diodes

Fensha Cai,[a] Yufei Tu,[b] Dadi Tian,[a] Yan Fang,[a] Bo Hou,[c] Muhammad Ishaq,[d] Xiaohong Jiang, [a] Meng Li, [a] Shujie Wang,[a] Zuliang Du*[a]*

[a] *Key Lab for Special Functional Materials of Ministry of Education, National & Local Joint Engineering Research Center for High-efficiency Display and Lighting Technology, School of Materials Science and Engineering, and Collaborative Innovation Center of Nano Functional Materials and Applications, Henan University, Kaifeng 475004, China*
E-mail: wsj@henu.edu.cn, zld@henu.edu.cn

[b] *School of Electronics Information and Intelligent Manufacturing, Sias University, Xinzheng, China*

[c] *School of Physics and Astronomy, Cardiff University, Cardiff, Wales, CF24 3AA, UK*

[d] *Institute of Fundamental and Frontier Sciences, University of Electronic Science and Technology of China, Chengdu 610054, China*

Abstract

Zinc oxide nanoparticles (ZnO NPs) have been actively pursued as the most effective electron transport layer for quantum-dot light-emitting diodes (QLEDs) in light of their unique optical, electronic properties and low-temperature processing. However, the high electron mobility and smooth energy level alignment at QDs/ZnO/cathode interfaces generate electron over-injection, which aggravates non-radiative Auger recombination. Meanwhile, the abundant defects (-OH and O_V) in ZnO NPs act as trap states inducing exciton quenching, which synergistically reduces the effective radiation recombination for degrading device performance. Here, we develop a bifunctional

surface engineering strategy to synthesize ZnO NPs with low defect density and high environmental stability by using ethylenediaminetetraacetic acid dipotassium salt (EDTAK) as an additive. The additive effectively passivates surface defects in ZnO NPs and induces chemical doping simultaneously. The bifunctional engineering leads to alleviate electron excess injection by elevating the conduction band level of ZnO to promote charge balance. As a result, state-of-the-art blue QLEDs with an EQE of 16.31% and a T_{50}@100 cd/m^2 of 1685 h are achieved, providing a novel and effective strategy to fabricate blue QLEDs with high efficiency and long operating lifetime.

1. Introduction

Quantum dot light-emitting diodes (QLEDs) featuring cost-effective electroluminescent, wide-color gamut and high-color purity are high-potential candidate for next-generation displays.[1-5] Indeed, progress in this area has been dramatic, the external quantum efficiency (EQE) of red, green and blue QLEDs has reached 30.9%, 28.7%, and 21.9%, respectively.[6,7] In addition, the T_{95} operating lifetimes (the time for the brightness to decrease to 95% of the initial brightness) of the three primary colors reached 7668, 7500 and 57 h at an initial brightness of 1000 cd m^{-2}, respectively.[7,8] Obviously, the performance of blue QLEDs is lower than their green and red counterparts. The main reason is that the deep valence band levels of the blue QDs emitting layer (EML) increase the hole injection barrier, thus leading to an imbalance of holes and electrons. Unbalanced carrier injection induces Auger recombination, thus affecting device efficiency and lifetime. Therefore, it is indispensable to achieve both high-efficiency and long-lifetime blue QLEDs.

For the state-of-the-art QLEDs device, ZnO NPs are the most commonly employed as electron transport layer (ETL) because of their high electron mobility and optimal energy band alignment.[9-11] However, QLEDs with ZnO ETL generally lead to charge imbalance in the QDs due to a non-negligible energetic barrier for holes injection. Consequently, the over-accumulation of electrons at the HTL/QDs interface leads to increasing non-radiative Auger recombination.[12] Additionally, low-temperature processed ZnO NPs exhibit a relatively open hexagonal close-packed lattice structure with the Zn atoms occupying only half of the tetrahedral sites, which therefore lead to Zn interstitials (Zn_I) and oxygen vacancies (O_V) trap states.[13,14] Previous reports revealed that residual hydroxyl group (-OH) defects exist on the surface of ZnO NPs during the solution process.[15] All these defects could act as charge-trapping centers, resulting in exciton quenching at the interface of the QDs/ETL interface.[16,17]

In view of the aforementioned issues, various strategies have been proposed to balance the charge injection and suppress interfacial exciton quenching. For instance: inserting insulating layers such as poly(methylmethacrylate) (PMMA),[18] poly-[(9,9-bis(30-(N,N-dimethylamino) propyl)-2,7-fluorene)-alt-2,7-(9,9-ioctylfluorene)] (PFN),[19] Al_2O_3 [20] and polyethylenimine (PEI)[21] between QDs and ETL; doping ZnO NPs with metals element including Mg,[22] Li,[23] Al,[24] Sn,[25] Be,[26] and Ga;[27] and altering the surface of ZnO NPs with organic materials.[28-31] Although these strategies can improve the device performance, it is challenging to precisely adjust the thickness of the ultrathin interlayer. A thin interlayer is ineffective in blocking electrons and can even have tunneling effects that promote electron injection. A thick interlayer increases resistance

and isolates charge transport. In addition, doped ZnO NP solutions appear to be particularly chemically reactive and have a propensity to agglomerate in the environment.[32] Therefore, in order to reduce electron over-injection and improve stability, techniques that can simultaneously control energy levels and passivate defects in ZnO NPs must be developed.

Here, we present a bifunctional strategy that uses EDTAK to tailor ZnO (EK-ZnO) as ETL in bule-QLEDs with improved efficiency and operational stability. The detailed analysis indicates that EDTAK can significantly passivate -OH and O_V defects to relieve exciton quenching. The chemical interaction contributes to upshifting the conduction band minimum (CBM) of ZnO to impede the injection of excess electrons. Meanwhile, the stability of ZnO NPs is increased due to the chelation function of EDTAK. Utilizing such bifunctional EK-ZnO as ETL, the fabricated QLED displays peak luminance values of 20060 cd/m^2 and EQE values of 16.31%. Peak values and EQE both improved by 42% and 53% over the control device, respectively. The device operating stability (T_{50}@100 cd m^{-2}) is enhanced by 10-folds from 170 h to 1685 h. The proposed strategy in this manuscript highlights the enormous potential for developing highly reliable and efficient QLEDs and other optoelectronic devices.

2. Result and Discussion

ZnO NPs were synthesized by the sol-gel method according to our previous work.[22] Typically, a zinc acetate dihydrate ($Zn(OAc)_2$•$2H_2O$) in dimethyl sulfoxide (DMSO) solution was mixed with tetramethylammonium hydroxide (TMAH) in ethanol solution.

The mixture was stirred for 1 hour to generate the ZnO nanocrystals, followed by precipitating with a mixed solution of ethanol and n-hexane then re-dispersed in ethanol. Regarding the EK-ZnO NPs, a EDTAK in methyl alcohol solution was added (Fig. S1) in the mixed solution of $Zn(OAc)_2•2H_2O$ and TMAH. The solution was stirred for 1 hour and re-dispersed in ethanol. (Details are shown in the Experimental Section). The presence of N1s and K 2p peak for EK-ZnO sample from X-ray photoelectron spectroscopy (XPS) measurements (Fig. 1a, S2) confirmed the incorporation of additives on the surface of the functionalized ZnO films.[33] An obvious red-shift absorption spectrum of EK-ZnO NPs in Fig. 1b authenticates the doping of K^+ in ZnO NPs. The acquired K^+ doping also caused a little increase in the grain size of ZnO NPs (from 4.23 nm to 4.37 nm), which might be assigned to the occupation of O_V in ZnO NPs by K^+,[35] as seen in TEM measurement (Fig. S3). Fourier transform infrared (FTIR) spectra was performed to further investigate the chemical interaction between ZnO and EDTAK. The peak around 2960 cm^{-1} corresponding to the C-H stretching vibration in EDTAK molecules was observed in EK-ZnO, indicating additives successful introduction of additives in ZnO film (Fig. S4).[34] The peak around 1641.3 cm^{-1} in EDTAK corresponded to C = O stretching vibration, while it disappeared in EK-ZnO. The stretching vibration of O-C-O also manifested as an additional peak at 1590.4 cm−1 (Fig. 1c).[31, 35] The conversion from C = O to O-C-O stretching vibration demonstrated a significant reduction of oxygen-bearing groups such as -OH group.[31] As the previous literature report, the -OH group binding to one metal site showed a basic characteristic, the -COOH group from EDTAK showed an acidic characteristic.[15, 33] Therefore, an

acid-base neutralization reaction occurred, reducing oxygen-containing groups like -OH on the surface of ZnO NPs. A typical wurtzite-type ZnO structure can be seen in XRD patterns of ZnO and EK-ZnO NPs (Fig. 1d). The absence of any peak shifts and additive peaks in EK-ZnO films demonstrating a small amount of additive accumulation in EK-ZnO films.[34]

Furthermore, atomic force microscopy (AFM) was carried out to study the surface topography of ZnO and EK-ZnO film surfaces deposited on bare glass. As shown in Fig. S5, the root-mean-square (RMS) values of both samples show negligible changes, suggesting a uniform coverage of the surface of ZnO films with no agglomeration and pinhole-free.

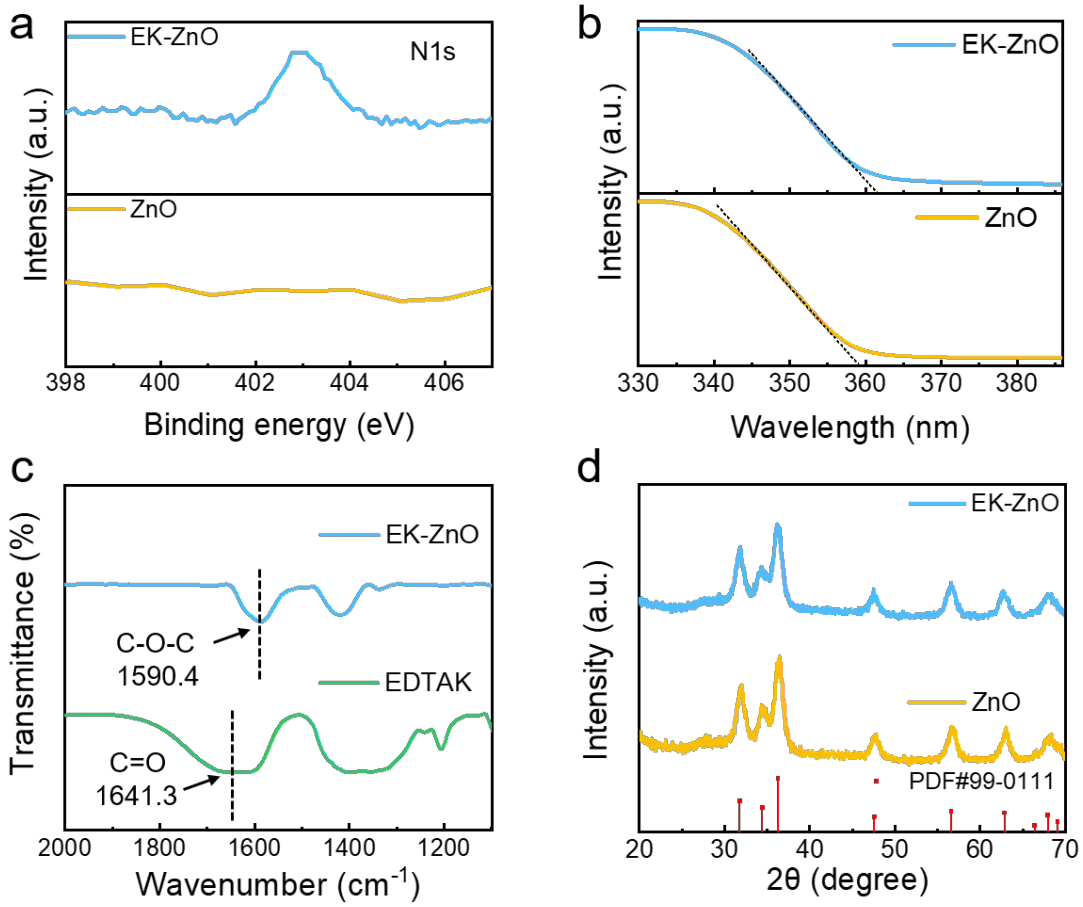

Fig. 1. (a) XPS spectra of N 1s, (b) UV-vis absorption spectra, (c) FTIR spectra and (d) XRD patterns of ZnO and EK-ZnO films.

To investigate the passivation effect of additive molecules on typical defects such as -OH and O_V of ZnO NPs, we characterized the steady state PL of ZnO and EK-ZnO solutions. The PL emission peaks around 375 nm is ascribed to near-band-edge emission, which is originated from intrinsic luminescence of ZnO exciton recombination.[22, 29] The peaks around 524 nm is ascribed to defect state emission such as O_V, -OH and interstitial oxygen generated during the synthesis.[36] The defect state emission may originated from the photo-excited electrons in the CBM of ZnO relax to the mid-gap defect states and recombine radiatively to the holes in the valence band .[37] The defect state emission intensity could reflect the density of defect states to a certain degree.[38] According to Fig. 2a, the additive molecules could successfully passivate the defects and lower the defect density in ZnO NPs by reducing the PL intensity of defect state emission and increasing near-band-edge emission (375 nm).

To further elucidate the defect's passivation effect, we performed X-ray photoemission spectroscopy (XPS) to analyze the binding energy of Zn 2p and O 1s core levels before and after EDTAK modification. As shown in Fig. 2b, O ls core level spectra are deconvoluted with Gaussian peaks for identifying the change after modification with EDTAK. Both pristine ZnO and EK-ZnO surfaces exhibit a peak at ~530.0 eV corresponding to the metal oxide (O_M). The shoulders at ~531.4 and ~532.0 eV are assigned to O_V and O_{OH}, respectively.[30, 34, 39] The percentages for these species are summarized in Fig. 2c, which clearly shows that both O_V and O_{OH} attenuate distinctly, accompanied by an increase in O_M. The XPS results and FTIR analyses demonstrated the deprotonation of carboxyl in EDTAK reacted with the surface-OH defects and K-

doped passivation of the O_V defects. Notably, the Zn 2p peaks of EK-ZnO presented a slight shift to lower binding energy compared with the unmodified samples, further suggesting a chemical interaction between the ZnO layer and additive molecules.[31]

To confirm the defects passivation effects, we performed steady-state PL and time-resolved PL decay (TRPL) measurements for QD films on quartz, ZnO and EK-ZnO substrates, respectively. QD films on ZnO and EK-ZnO exhibited weaker PL emission compared with those on quartz, consistent with the exciton quenching at QDs/ZnO interface by defect capturing. The quartz/QDs/EK-ZnO sample showed stronger PL emission than quartz/QDs/ZnO sample. This implies reduced quenching of QDs at the interface resulting increased radiative recombination. The average exciton lifetime (τ_{avg}), was extracted by a bi-exponential fitting function.[40] The τ_{avg} was rapidly reduced to 4.35 ns for quartz/QDs/ZnO relative to 5.88 ns for quartz/QDs, and then the τ_{avg} was gradually increased to 5.13 ns in EK-ZnO sample (Table S1) indicating that the present additives were effective in suppressing the interfacial non-radiative recombination at QDs/ZnO interface.

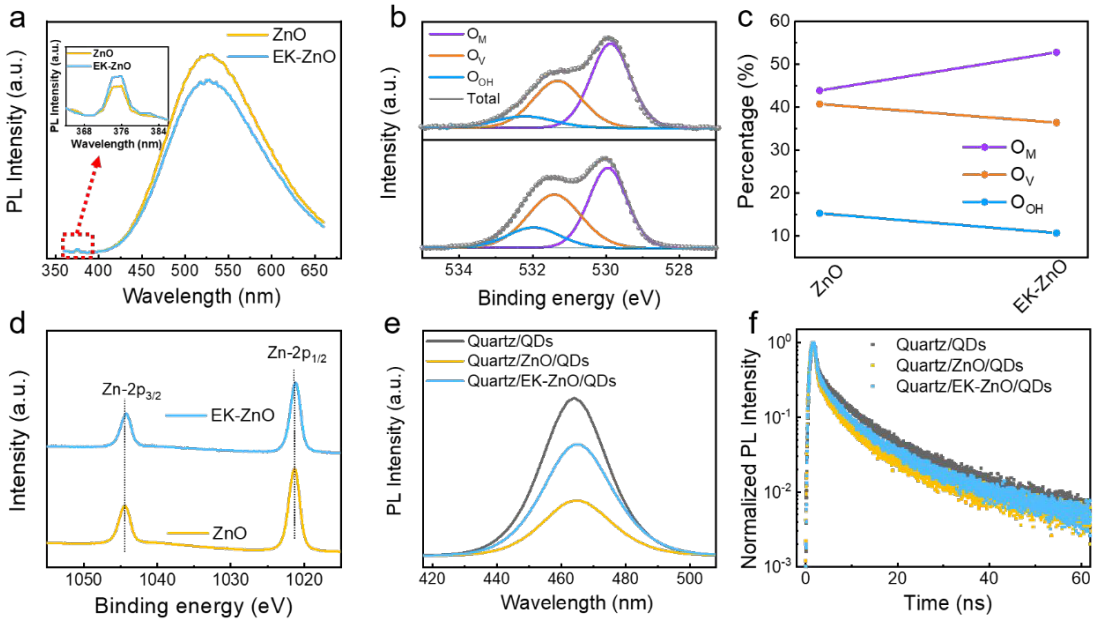

Fig. 2. (a) Steady-state PL spectra of ZnO and EK-ZnO solution, inset: locally amplified PL spectrum in the ultraviolet region. XPS spectra of (b) O 1s (d) Zn 2p ZnO and EK-ZnO films. (c) The percentages of O_{OH}, O_V, and O_M extracted from the XPS spectra of O 1s results. (e) Steady-state PL spectrum and (f) time-resolved PL decay curves of QD films on quartz, ZnO and EK-ZnO substrates.

Based on these observations, the passivation effect was attributed to the chemical interaction between the ZnO layer and additive molecules. Reducing surface -OH defects via acid-base neutralization reaction and O_V defects induced by K^+ doping into ZnO simultaneously, which will tune the energy-level alignment at this interface.[33, 34] These changes were revealed by UV-vis absorption spectra and ultraviolet photoemission spectroscopy (UPS) analysis.

The UV-vis absorption spectra demonstrate an optical bandgap (Eg) of 3.52 eV for ZnO and 3.49 eV for EK-ZnO, consistent with previous reports (Fig.3a).[41,42] Fig.3b shows the secondary photoelectron cutoff ($E_{cut-off}$) and valence band region (E_{onset}) for ZnO and EK-ZnO. The work functions (WF) of pristine ZnO and EK-ZnO were determined to be 3.80 and 3.53 eV, respectively, using the equation: $W_F = 21.22\text{-}E_{cutoff}$.[43] Combined with bandgap, the CBM of pristine ZnO and EK-ZnO were found to be -3.97 and -3.69

eV, respectively, which is demonstrated in the corresponding energy level diagram (Fig. 3c). An increased energy barrier for electron transport at the EK-ZnO/Al interface impedes the excessive electron injection and facilitated the charge balance in the device. Meanwhile, the CBM of EK-ZnO was slightly higher than that of QDs, that resulted in reduce space-electron accumulation at the QD/EK-ZnO interface, thereby suppressing the degradation at the QD-ETL junction to enhance the stability.[12] Fig. S6 exhibits the UPS spectra of QDs film on ITO, for which the CBM and valence band maximum are 3.71 and 6.47 eV, respectively. A single-carrier device of electron-only devices (EODs) with a structure of ITO/ETL/QDs/ETL/Al and the hole-only devices (HODs) with a structure of ITO/PEDOT/PF8Cz/QDs/MoO_3/Al were prepared to verify this hybrid configuration (Fig. 3d). The electron current decreased by a unity order of magnitude in EK-ZnO-based QLEDs, much closer to the hole current compared with ZnO-based devices. These results indicate that the upshift CBM of ZnO by additives treatment promotes the balance of charge injection in the QDs.

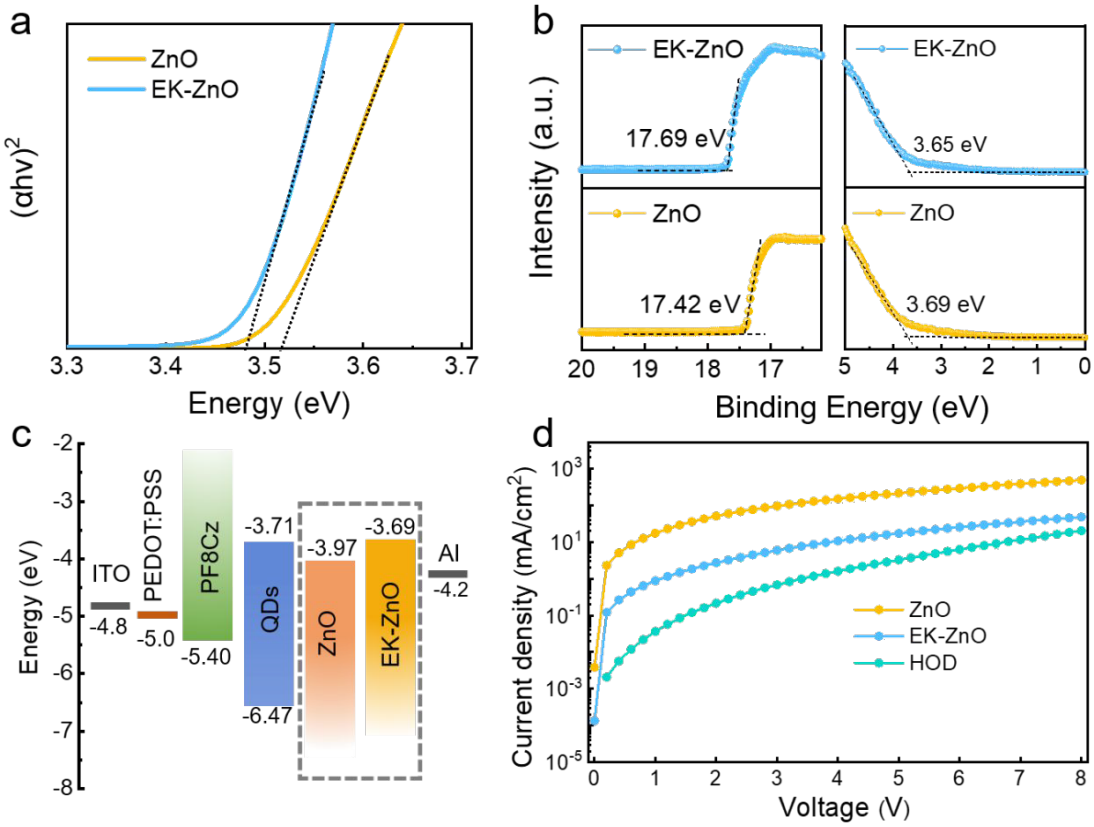

Fig. 3. (a) Tauc plots and (b) UPS spectra of ZnO and EK-ZnO films. (c) Schematic energy level diagram. (d) Current density-voltage characteristics of electron-only and hole-only devices.

For further assessment of EDTAK modified ZnO NPs effect on the device performance, blue QLEDs with the structure of ITO/PEDOT/PF8Cz/QDs/ETL/Al were also fabricated as demonstrated in Fig. 4a. CdSe/ZnSe/ZnS core/shell QDs with central emission wavelength of 459 nm with full width at half maximum (FWHM) of 25 nm was used as EML (Fig. S7a). The photoluminescent quantum yield (PLQY) is about 65%. Fig. S7b is the TEM image of CdSe/ZnSe/ZnS QDs with an average size of size of 10 nm. A normalized EL spectra of QLEDs driven under 3.2 V exhibit pure blue emission at 468 nm without any parasitic contribution from the other neighboring layers (Fig. 4b). The inset of Fig. 4b displays photos of QLEDs operating at 3.2 V, corresponding to the Commission Internationale de I'Eclairage color coordinates of

(0.129, 0.068). This illustrates that the charge transport layers have no effect on exciton radiative recombination. Notably, Fig. S8 and S9 exhibit EL spectra and CIE coordinates of our QLEDs with no obvious change from 2.6 to 5.0 V, indicating a substantial stability.

The current-voltage-luminance (*J-V-L*), EQE-luminance (*EQE-L*) and current efficiency-luminance (*CE-L*) characteristics of the QLEDs based on ZnO and EK-ZnO ETL exhibit lower current density compared with the ZnO-based devices (Fig. 4c, d). The results validated that the electron injection in EK-ZnO-based devices was less efficient compared with the ZnO-based devices, which was ascribed to the increased barrier for electron injection. A considerable increase in luminance due to restraining Auger recombination by excess electrons.[44] As a result, devices based on EK-ZnO ETL achieved a maximum luminance and peak EQE of 20060 cd/m^2 and 16.31%, respectively, which was remarkably higher than 14140 cd/m^2 and 10.67% of the ZnO ETL devices (Fig. 1d). The relevant device parameters were summarized in Table 1. Furthermore, a histogram of the maximum EQE of the optimized devices showed that an average EQE of the 18 devices was 15.68% with a low standard deviation of 0.64, suggesting high device reproducibility (Fig. S10). The operational T_{50} lifetime (when the luminance drops to 50% of its initial value) of EK-ZnO-based QLEDs was measured to be 5.05 h at an initial luminance of 3457 cd/m^2, equivalent to 1686 h at 100 cd/m^2 by applying an acceleration factor of 1.64 (Fig.4d).[5, 45] The enhanced T_{50} lifetime for the optimized devices is attributed to reduced Auger recombination and the improved stability of ZnO NPs by EDTAK chelation.[46] Additionally, the excellent

stability was revealed by the keeping the ZnO, where EK-ZnO solution in an ambient atmosphere with a relative humidity of 35-40% for 3 days, it was clear that the EK-ZnO solution remained clear while the ZnO sample become turbid (Fig. S11).

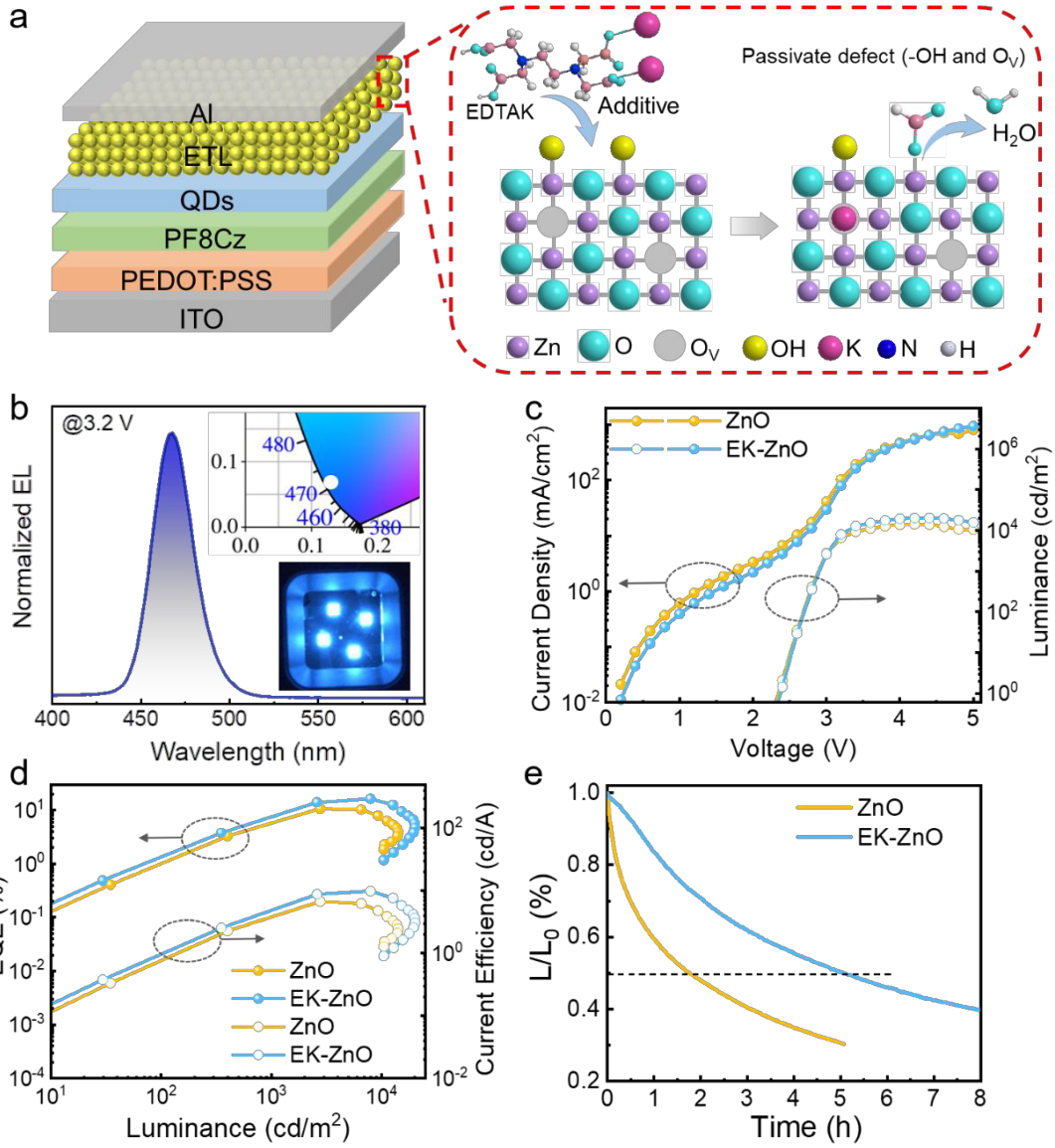

Fig. 4. Device performance. (a) Device structure and schematic illustration of EDTAK modify ZnO. (b) EL spectrum under 3.2 V bias. Inset: photographs of the operating devices and corresponding CIE coordinates. (c) Current density-luminance-voltage characteristics. (d) External quantum efficiency and current efficiency as a function of luminance for devices based on ZnO and EK-ZnO ETLs. (e) Operational stability data for the two devices.

Table 1. Summary EL Performance of QLEDs with ZnO and EK-ZnO ETLs.

Device	EL (nm)	V_{on} (V)	L_{MAX} (cd/m^2)	CE (cd/A)	PE (lm/W)	EQE (%)
ZnO	468	2.4	14140	6.76	7.08	10.67
EK-ZnO	468	2.4	20060	9.89	9.71	16.31

These systematic analysis and results concluded the improved efficiency of the QLEDs based on the EK-ZnO ETLs, which was attributed to the bifunctional engineering strategy on ZnO using EDTAK. Fig. S12 illustrates the schematic of performance enhancement for devices with primordial ZnO and additives-treatment ZnO films. In ZnO-based device, the electrons transfer barrier was smooth where excess electrons accumulate at PF8Cz/QDs interface, inducing non-radiative Auger recombination. In addition, the abundant defects (-OH and O_V) on the ZnO surface acted as trap states inducing exciton quenching, which synergistically reduced the radiation recombination ratio for degrading device performance. Similarly, for the QLED devices based on EK-ZnO ETL, the carboxyl in EDTAK significantly passivated -OH defects meanwhile doping K^+ ions passivated O_V in ZnO and the interfacial QDs/ETL, thus suppressing exciton quenching. The chemical interaction contributed to elevated conduction band energy level of ZnO, increased the electron injection barrier at ETL/Al cathode and alleviated the electron over-injection, facilitating charge balance. Therefore, the bifunctional surface engineering strategy synergistically enhanced the proportion of radiative recombination, resulting in improved device performance.

3. Conclusions

We report the fabrication of blue QLEDs with a high efficiency, high luminance, and

extended lifetime using ZnO NPs modified with EDTAK additives as ETLs. The surface engineering passivated the surface defects in ZnO NPs and raised the electron injection barrier energy level. These effects were well reflected in the device performance, which exhibited enhanced charge balance and inhibited exciton quenching, thus increasing effective radiation recombination of QDs. The QLEDs fabricated with EK-ZnO achieved an EQE of 16.31% with outstanding long-operational-lifetime. A remarkable lifetime achieved improved by suppressing the Auger recombination and the increased stability of ZnO. It is anticipated that this work identifies a new strategy for developing efficient and stable QLEDs for next-generation displays.

4. Experimental section

4.1. Materials and synthesis

Materials. All reagents and materials were used as received without any purification: zinc acetate dihydrate ($Zn(OAc)_2•2H_2O$, 99.99%), ethylenediaminetetraacetic acid dipotassium salt (EDTAK, 98%), n-octane (98%), dimethyl sulfoxide (DMSO, 99.7%) and tetramethylammonium hydroxide pentahydrate (TMAH, 97%) were purchased from Sigma Aldrich. The light emission layer (EML) of CdSe/ZnSe/ZnS core-shell QDs were purchased from Suzhou Xingshuo Nanotech Co., Ltd. The PL is 459 nm with a FWHM of 25 nm, and the PLQY is about 65%. The particle size is about 10 nm. Poly((9,9-dioctylfluorenyl-2,7-diyl)-alt-(9-(2-ethylhexyl)-carbazole-3,6-diyl)) (PF8Cz) was purchased from Dongguan Fuan Optoelectronics Technology Co., Ltd.

Synthesis of ZnO and EK-ZnO nanoparticles. $Zn(OAc)_2•2H_2O$ was dissolved in 30.0 mL of DMSO with the concentration of 0.1 M as solution A. Tetramethylammonium hydroxide (TMAH) was dissolved in ethanol with the concentration of 0.55 M as solution B. Added dropwise 10 mL solution B to solution A with a peristaltic pump, the flow rate is 0.47 mL/min. Then the solution was stirred for 1 h at 20 ~ 25 °C with the humidity of 30% to obtain ZnO NPs. Finally, ZnO NPs were centrifuged by using a mixed solution (1: 1.5) of ethanol and n-hexane with a speed of 3000 r/min for 4 min, and re-dispersed in absolute ethyl alcohol with a concentration of 20.0 mg/mL.

EK-ZnO nanoparticles. $Zn(OAc)_2•2H_2O$ was dissolved in 30.0 mL of DMSO with the concentration 0.1 M as solution A. TMAH was dissolved in ethanol with the concentration of 0.55 M as solution B. Added dropwise 10 mL solution B to solution A with the same speed of ZnO NPs. 0.8 mL EDTAK in methyl alcohol with the concentration of 1 mM was added in the mixed solution of A and B with the flow rate is 0.47 mL/min. Stirred for 1 h at 20 ~ 25 °C with the humidity of 30% to obtain EK-ZnO NPs. EK-ZnO NPs were centrifuged and re-dispersed with the same methods of ZnO NPs, and the concentration was kept 20.0 mg/mL .

4.2. Fabrication of QLEDs. The device structure was glass/ITO/PEDOT:PSS/PF8Cz/QDs/ETLs/Al. The patterned ITO coated glass substrates with a sheet resistance of 23 Ω/sq were thoroughly cleaned ultrasonically in detergent, deionized water, acetone, and isopropanol for 30 min and then dried, respectively. After cleaning, the ITO glasses were treated with UV-ozone for 15 min.

After UV-ozone treatment, poly(3,4-ethylenedioxythiophene)/poly(styrene sulfonate) (PEDOT:PSS, AI 4083) solution with the solid content of 1.4% in water was spin-coated on the ITO substrates at 5000 rpm for 45 s and annealed at 140 °C for 15 min. Then, the substrates were transferred into a N_2-filled glovebox. Subsequently, PF8Cz (8.0 mg/mL in chlorobenzene) hole transport layer was spin-coated onto the PEDOT:PSS layer at 3000 rpm for 30 s and thermally annealed at 150 °C for 30 min. The CdSe/ZnSe/ZnS core-shell QDs dispersed in n-octane (18.0 mg/mL) and ETLs (ZnO or EK-ZnO NPs 20.0 mg/mL) were spin-coated at 3000 rpm for 30 s and baked at 60 °C for 30 min. Finally, the device was transferred to vacuum chamber having a pressure of 5×10^{-6} Torr for Al cathode (100 nm) evaporation. After fabrication, the devices were encapsulated with UV-resin (NOA61 from Norland) inside the N_2-filled glovebox. The cover glass was mounted on top of the QLED with UV-resin and then they were cured under intense UV radiation for 1 min. The active area of each device is 0.04 cm^2.

4.3. Characterization methods

Current density-voltage-luminance and the EQE characteristics of blue QLEDs were performed using a characterization system comprising a Keithley 2400 voltmeter together with a Photo Research 735 (PR-735) spectroradiometer under ambient conditions. The XPS measurement was performed via AXIS SUPRA+ System (Shimadzu Inc.) equipped with monochromatic Al Ka X-ray photons (1486.6 eV) radiation. The absorption was measured using a Lambda 950 PerkinElmer spectrometer.

PL and TRPL spectra were performed on a HORIBA FluoroLog-3 spectrofluorometer, respectively. AFM morphology and KPFM were carried out by a SPA400 atomic force microscope. UPS spectra were acquired with a Thermo Scientific ESCALAB 250 Xi surface-analysis system with a He I discharge lamp (21.22 eV). The operational lifetime T_{50} of the devices was measured by a QLED life test system of Newport Keithley N6705B.

Author Contributions

Zuliang Du, Meng Li and Shujie Wang conceived the idea and proposed the experimental setup. Fensha Cai carried out the initial experimental work, characterization, analyzed the data, and wrote the original draft of the manuscript. Yan Fang, Meng Li and Xiaohong Jiang instructed the experiments. Yufei Tu and Dadi Tian contributed to optimize the various experimental steps. Bo Hou and Muhammad Ishaq revised the manuscript. Zuliang Du and Yufei Tu provided financial supports and other necessary research resources. All authors reviewed the manuscript and discussed the results.

Conflicts of interest

There are no conflicts to declare.

Acknowledgements

The authors would like to thank the financial support from the National Natural Science

Foundation of China (Grant No. U1604261), Key Scientific Research Project in Colleges and Universities of Henan Province of China (Grant No. 21A416001), Key Technologies R&D Program of Henan (Grant No. 232102231038).

References

1 D. Tian, H. Ma, G. Huang, M. Gao, F. Cai, Y. Fang, C. Li, X. Jiang, A. Wang, S. Wang, Z. Du, *Adv. Opt. Mater.,* 2022, **11**, 2201965-2201982.

2 B. Li, M. Lu, J. Feng, J. Zhang, P. M. Smowton, J. I. Sohn, I.-K. Park, H. Zhong, B. Hou, *J. Mater. Chem. C,* 2020, **8**, 10676-10695.

3 A. R. C. Osypiw, S. Lee, S.-M. Jung, S. Leoni, P. M. Smowton, B. Hou, J. M. Kim, G. A. J. Amaratunga, *Mater. Adv.,* 2022, **3**, 6773-6790.

4 M. Liu, N. Yazdani, M. Yarema, M. Jansen, V. Wood, E. H. Sargent, *Nat. Electron.,* 2021, **4**, 548-558.

5 H. Shen, Q. Gao, Y. Zhang, Y. Lin, Q. Lin, Z. Li, L. Chen, Z. Zeng, X. Li, Y. Jia, S. Wang, Z. Du, L. S. Li, Z. Zhang, *Nat. Photonics,* 2019, **13**, 192-197.

6 J. Song, O. Wang, H. Shen, Q. Lin, Z. Li, L. Wang, X. Zhang, L. S. Li, *Adv. Funct. Mater.,* 2019, **29**, 1808377-1808385.

7 Y. Deng, F. Peng, Y. Lu, X. Zhu, W. Jin, J. Qiu, J. Dong, Y. Hao, D. Di, Y. Gao, T. Sun, M. Zhang, F. Liu, L. Wang, L. Ying, F. Huang, Y. Jin, *Nat. Photonics,* 2022, **16**, 505-511.

8 D. Liu, S. Cao, S. Wang, H. Wang, W. Dai, B. Zou, J. Zhao, Y. Wang, *J. Phys. Chem. Lett.,* 2020, **11**, 3111-3115.

9 B.-Y. Lin, W.-C. Ding, C.-H. Chen, Y.-P. Kuo, P.-Y. Chen, H.-H. Lu, N. Tierce, C. J. Bardeen, J.-H. Lee, T.-L. Chiu, C.-Y. Lee, *Chem. Eng. J.,* 2021, **417**, 127983-127990.

10 P. Yu, Q. Yuan, J. Zhao, H. Zhang, W. Ji, *J. Phys. Chem. Lett.,* 2022, **13**, 2878-2884.

11 L. Qian, Y. Zheng, J. Xue, P. H. Holloway, *Nat. Photonics,* 2011, **5**, 543-548.

12 S. Chen, W. Cao, T. Liu, S. W. Tsang, Y. Yang, X. Yan, L. Qian, *Nat. Commun.,* 2019, **10**, 765-773.

13 M. A. Mahmud, N. K. Elumalai, M. B. Upama, D. Wang, A. M. Soufiani, M. Wright, C. Xu, F. Haque, A. Uddin, *ACS Appl. Mater. Interfaces,* 2017, **9**, 33841-33854.

14 L. S.-M. a. J. L. MacManus-Driscoll, *Mater. Today,* 2007, **10**, 40-48.

15 E.-H. Jung, B. Chen, K. Bertens, M. Vafaie, S. Teale, A. Proppe, Y. Hou, T. Zhu, C. Zheng, E. H. Sargent, *ACS Energy Lett.,* 2020, **5**, 2796-2801.

16 Q. Su, Y. Sun, H. Zhang, S. Chen, *Adv. Sci.,* 2018, **5**, 1800549-1800555.

17 W. Zhang, X. Chen, Y. Ma, Z. Xu, L. Wu, Y. Yang, S. W. Tsang, S. Chen, *J. Phys. Chem. Lett.,* 2020, **11**, 5863-5870.

18 X. Dai, Z. Zhang, Y. Jin, Y. Niu, H. Cao, X. Liang, L. Chen, J. Wang, X. Peng,

Nature, 2014, **515**, 96-99.
19 J. Lim, W. K. Bae, D. Lee, S. Lee, C. Lee, K. Char, *ACS Nano,* 2013, **7**, 9019-9026.
20 H. Zhang, N. Sui, X. Chi, Y. Wang, Q. Liu, H. Zhang, W. Ji, *ACS Appl. Mater. Interfaces,* 2016, **8**, 31385-31391.
21 K. Ding, H. Chen, L. Fan, B. Wang, Z. Huang, S. Zhuang, B. Hu, L. Wang, *ACS Appl. Mater. Interfaces,* 2017, **9**, 20231-20238.
22 S. Wang, Y. Guo, D. Feng, L. Chen, Y. Fang, H. Shen, Z. Du, *J. Mater. Chem. C,* 2017, **5**, 4724-4730.
23 H. M. Kim, J. Kim, S. Y. Cho, J. Jang, *ACS Appl. Mater. Interfaces,* 2017, **9**, 38678-38686.
24 Y. Sun, W. Wang, H. Zhang, Q. Su, J. Wei, P. Liu, S. Chen, S. Zhang, *ACS Appl. Mater. Interfaces,* 2018, **10**, 18902-18909.
25 V. Postica, J. Gröttrup, R. Adelung, O. Lupan, A. K. Mishra, N. H. de Leeuw, N. Ababii, J. F. C. Carreira, J. Rodrigues, N. B. Sedrine, M. R. Correia, T. Monteiro, V. Sontea, Y. K. Mishra, *Adv. Funct. Mater.,* 2017, **27**, 1604676-1604690.
26 A. Chen, H. Zhu, Y. Wu, M. Chen, Y. Zhu, X. Gui, Z. Tang, *Adv. Funct. Mater.,* 2016, **26**, 3696-3702.
27 S. Cao, J. Zheng, J. Zhao, Z. Yang, C. Li, X. Guan, W. Yang, M. Shang, T. Wu, *ACS Appl. Mater. Interfaces,* 2017, **9**, 15605-15614.
28 Y. Han, H. Dong, W. Pan, B. Liu, X. Chen, R. Huang, Z. Li, F. Li, Q. Luo, J. Zhang, Z. Wei, C. Q. Ma, *ACS Appl. Mater. Interfaces,* 2021, **13**, 17869-17881.
29 J. Wei, G. Ji, C. Zhang, L. Yan, Q. Luo, C. Wang, Q. Chen, J. Yang, L. Chen, C. Q. Ma, *ACS Nano,* 2018, **12**, 5518-5529.
30 S. Bai, Y. Jin, X. Liang, Z. Ye, Z. Wu, B. Sun, Z. Ma, Z. Tang, J. Wang, U. Würfel, F. Gao, F. Zhang, *Adv. Energy Mater.,* 2015, **5**, 1401606-1401615.
31 Z. Wang, X. Zhu, J. Feng, C. Wang, C. Zhang, X. Ren, S. Priya, S. F. Liu, D. Yang, *Adv. Sci.,* 2021, **8**, 2002860-2002866.
32 X. Liang, S. Bai, X. Wang, X. Dai, F. Gao, B. Sun, Z. Ning, Z. Ye, Y. Jin, *Chem. Soc. Rev.,* 2017, **46**, 1730-1759.
33 Z. Liu, L. Qiu, L. K. Ono, S. He, Z. Hu, M. Jiang, G. Tong, Z. Wu, Y. Jiang, D.-Y. Son, Y. Dang, S. Kazaoui, Y. Qi, *Nature Energy,* 2020, **5**, 596-604.
34 X. Z. Dan Zhang, Tonghui Guo, Junjie Zou, Yuan Zhou, Junjun Jin, Zhenkun Zhu, Qiang Cao, Jing Zhang, and Qidong Tai, *Small,* 2022, **19**, 2205604-2205614.
35 D. Yang, R. Yang, K. Wang, C. Wu, X. Zhu, J. Feng, X. Ren, G. Fang, S. Priya, S. F. Liu, *Nat. Commun.,* 2018, **9**, 3239-3349.
36 M. Gao, Y. Tu, D. Tian, H. Yang, X. Fang, F. Zhang, H. Shen, Z. Du, *ACS Photonics,* 2022, **9**, 1400-1408.
37 Ü. Özgür, Y. I. Alivov, C. Liu, A. Teke, M. A. Reshchikov, S. Doğan, V. Avrutin, S. J. Cho, H. Morkoç, *J. Appl. Phys.,* 2005, **98**, 041301-041413.
38 J. H. Lin, R. A. Patil, R. S. Devan, Z.-A. Liu, Y.-P. Wang, C.-H. Ho, Y. Liou, Y.-R. Ma, *Sci. Rep.,* 2014, **4**, 6967-6974.

39 M. Chrzanowski, G. Zatryb, P. Sitarek, A. Podhorodecki, *ACS Appl. Mater. Interfaces,* 2021, **13**, 20305-20312.
40 J. Wu, L. Chen, Y. Zhao, Z. Xiong, W. Ji, Y. Lei, *Appl. Phys. Lett.,* 2021, **119**, 073303-073308.
41 R. Azmi, S. Hwang, W. Yin, T.-W. Kim, T. K. Ahn, S.-Y. Jang, *ACS Energy Lett.,* 2018, **3**, 1241-1246.
42 K. Karmakar, A. Sarkar, K. Mandal, G. G. Khan, *Chem. Electro. Chem.,* 2018, **5**, 1147-1152.
43 J. Zhang, H. Yu, *J. Mater. Chem. A,* 2021, **9**, 4138-4149.
44 Q. Lin, L. Wang, Z. Li, H. Shen, L. Guo, Y. Kuang, H. Wang, L. S. Li, *ACS Photonics,* 2018, **5**, 939-946.
45 T. Lee, B. J. Kim, H. Lee, D. Hahm, W. K. Bae, J. Lim, J. Kwak, *Adv. Mater.,* 2022, **34**, 2106276-2106284.
46 T. Fang, T. Wang, X. Li, Y. Dong, S. Bai, J. Song, *Sci. Bull.,* 2021, **66**, 36-43.

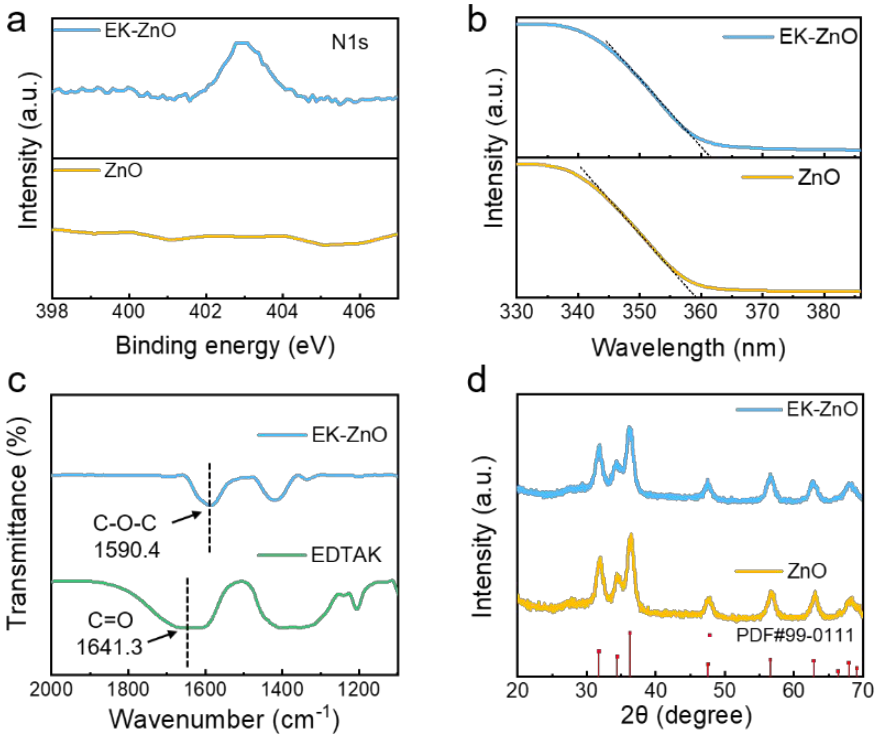

Fig. 1. (a) XPS spectra of N 1s, (b) UV-vis absorption spectra, (c) FTIR spectra and (d) XRD patterns of ZnO and EK-ZnO films.

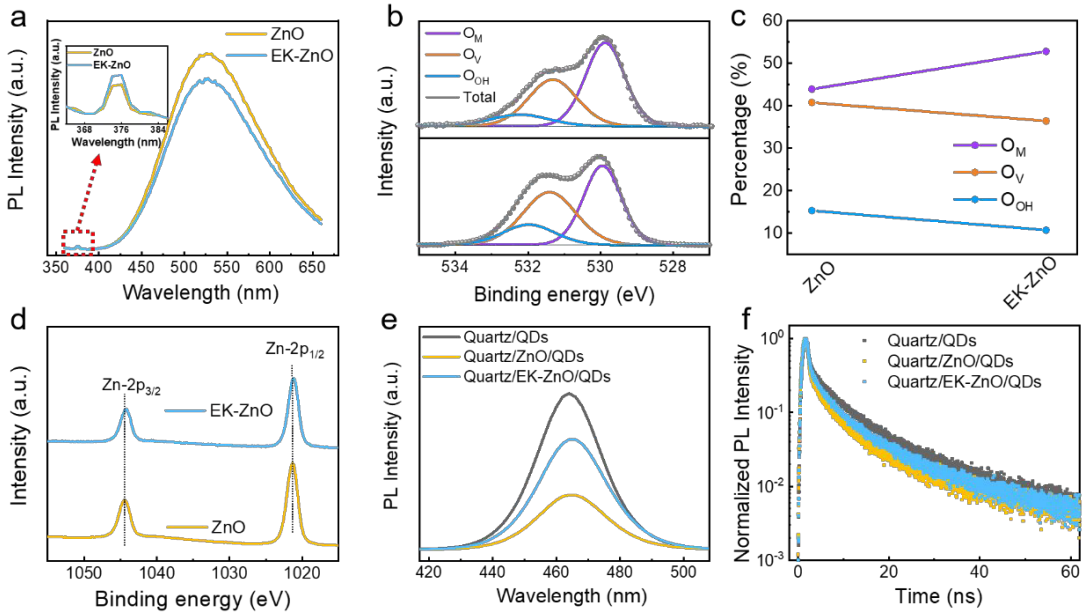

Fig. 2. (a) Steady-state PL spectra of ZnO and EK-ZnO solution, inset: locally amplified PL spectrum in the ultraviolet region. XPS spectra of (b) O 1s (d) Zn 2p ZnO and EK-ZnO films. (c) The percentages of O_{OH}, O_V, and O_M extracted from the XPS spectra of O 1s results. (e) Steady-state PL spectrum and (f) time-resolved PL decay curves of QD films on quartz, ZnO and EK-ZnO substrates.

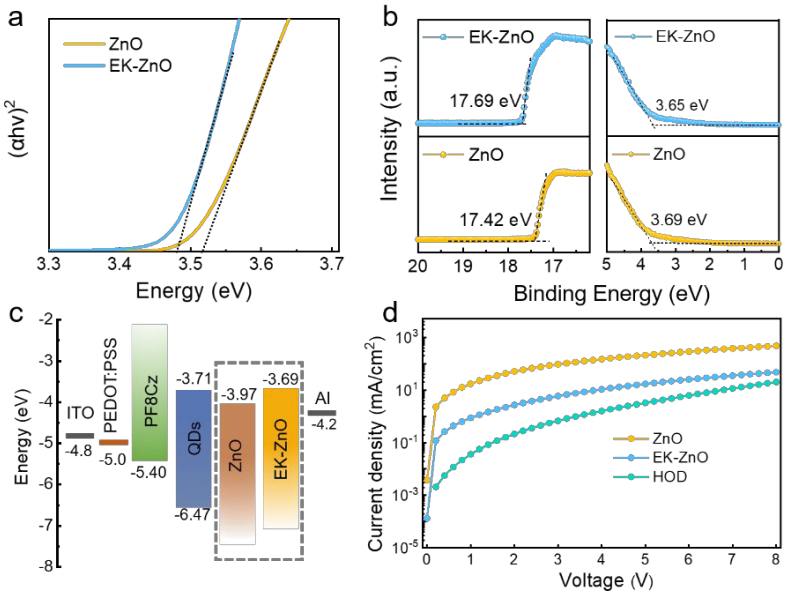

Fig. 3. (a) Tauc plots and (b) UPS spectra of ZnO and EK-ZnO films. (c) Schematic energy level diagram. (d) Current density-voltage characteristics of electron-only and hole-only devices.

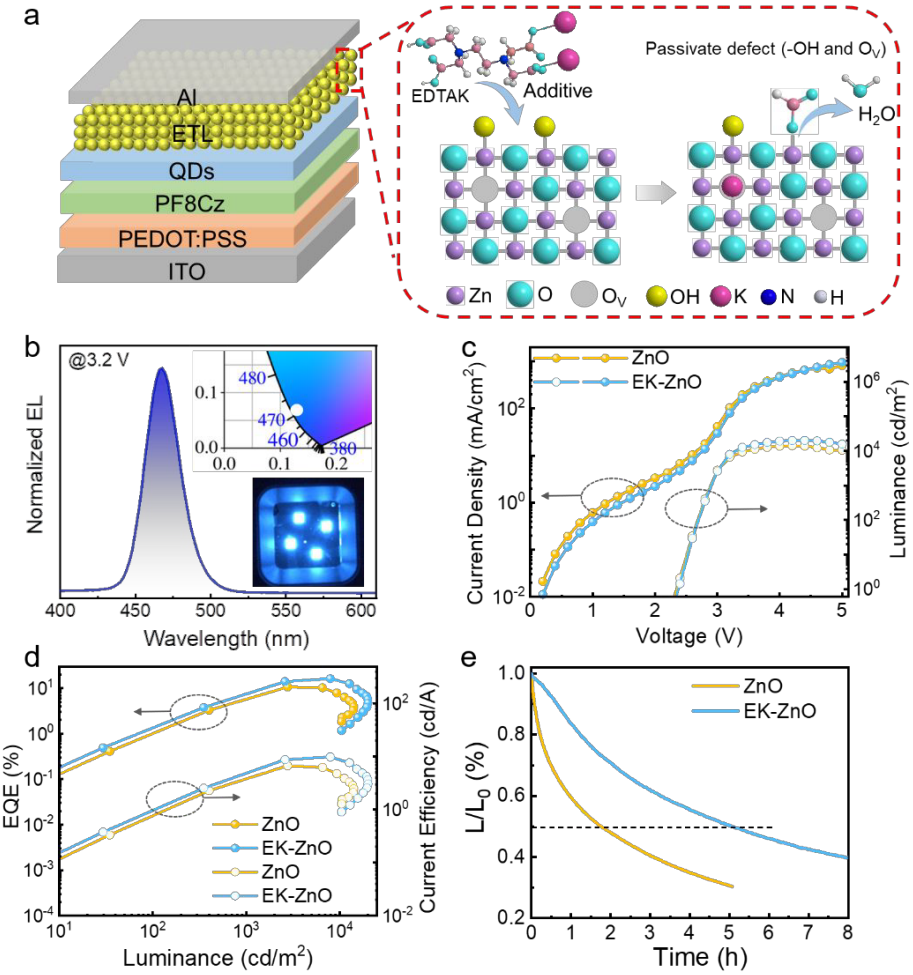

Fig. 4. Device performance. (a) Device structure and schematic illustration of EDTAK modify ZnO. (b) EL spectrum under 3.2 V bias. Inset: photographs of the operating devices and corresponding CIE coordinates. (c) Current density-luminance-voltage characteristics. (d) External quantum efficiency and current efficiency as a function of luminance for devices based on ZnO and EK-ZnO ETLs. (e) Operational stability data for the two devices.

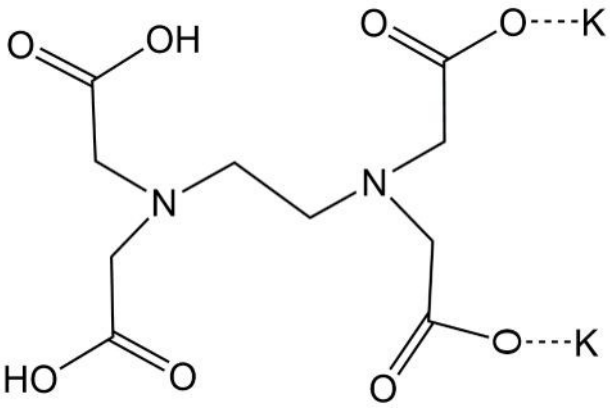

Fig. S1 Molecular structures of EDTAK.

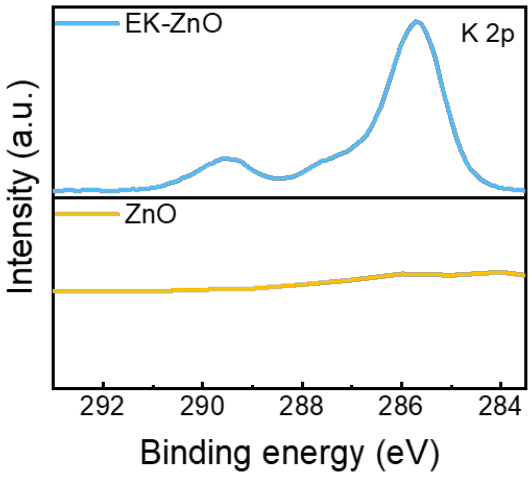

Fig. S2 XPS spectra of K 2p.

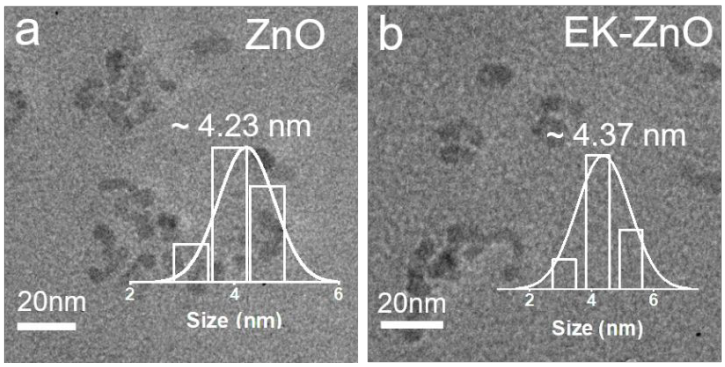

Fig. S3 TEM images of ZnO and EK-ZnO NPs. Insets, corresponding size distribution histogram.

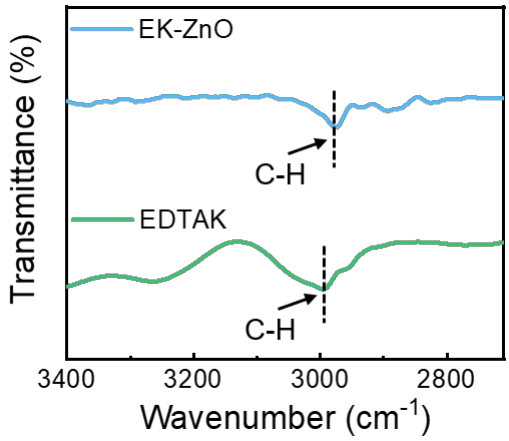

Fig. S4 FTIR of EDTAK and EK-ZnO NPs.

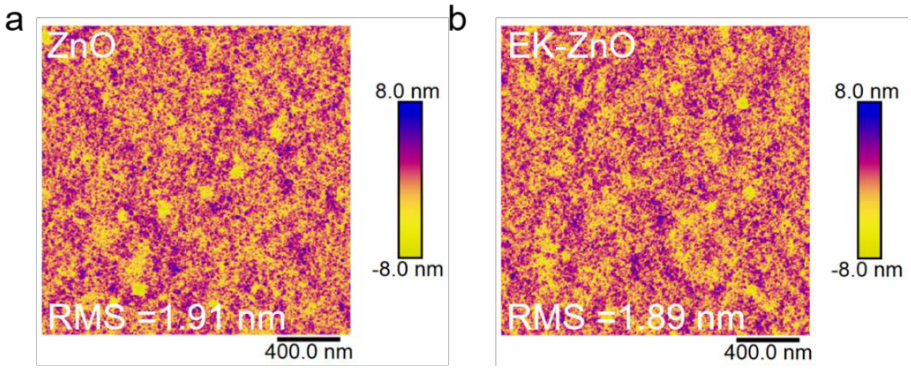

Fig. S5 AFM images of ZnO and EK-ZnO films on glass substrate.

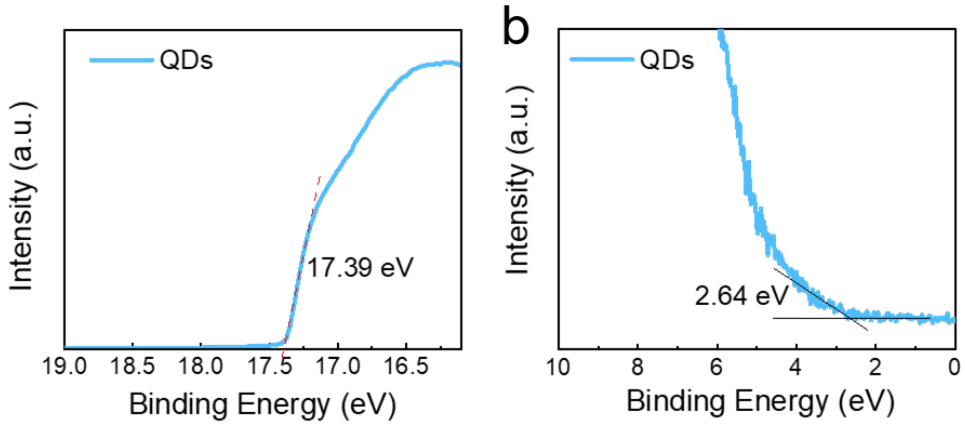

Figure S6. UPS spectra of QDs film on ITO.

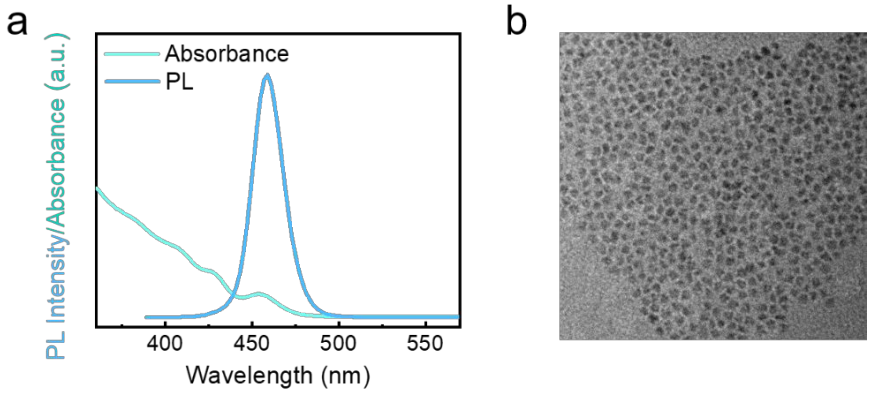

Fig. S7 (a) UV-vis absorption and PL spectra of the CdSe/ZnSe/ZnS QDs. (b) TEM image of CdSe/ZnSe/ZnS QDs.

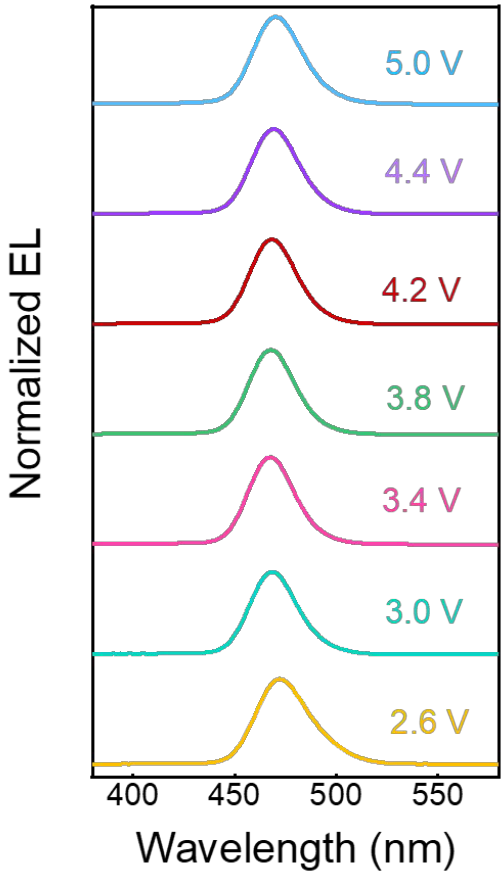

Fig. S8 EL spectra of the QLED with EK-ZnO under an applied voltage of 3.0-5.0 V.

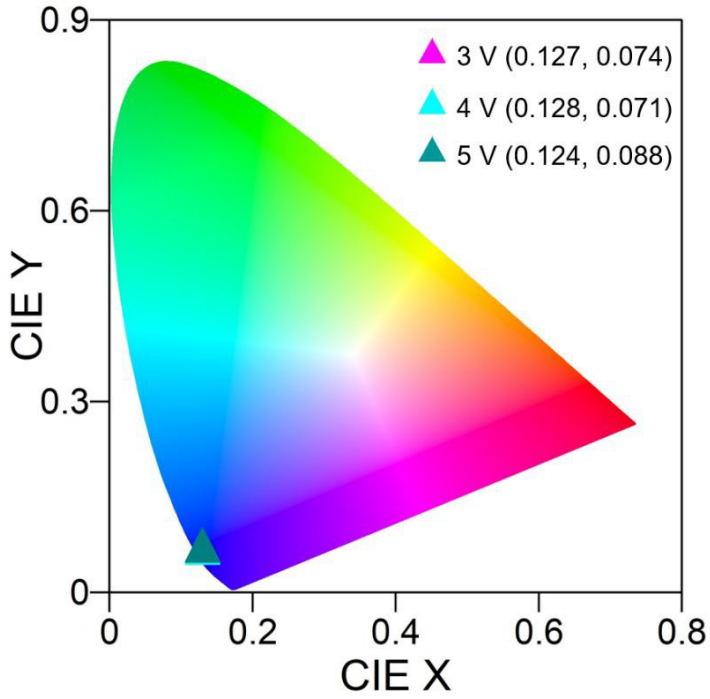

Fig. S9 CIE coordinates of QLEDs based on EK-ZnO ETL under an applied voltage of 3.0-5.0 V.

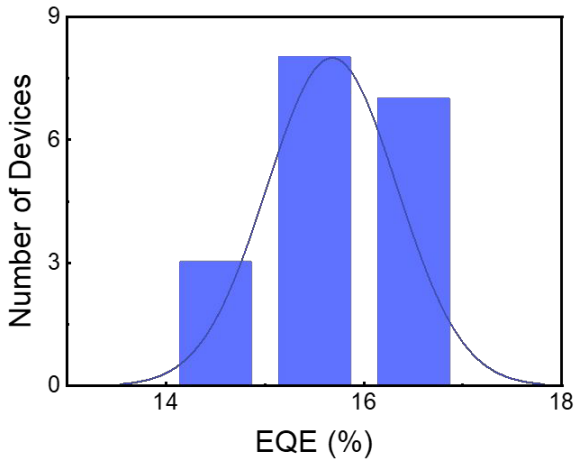

Fig. S10 EQE histogram of 18 devices based on EK-ZnO ETL. The fitting curve is a distribution function curve.

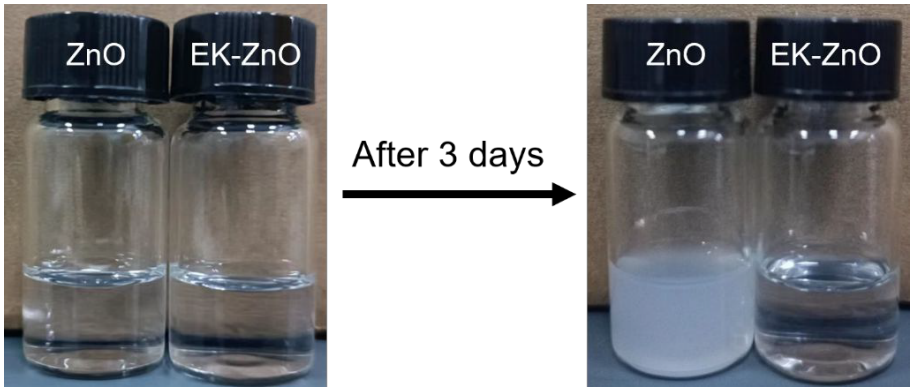

Fig. S11 Photo-graphs of ZnO and EK-ZnO nanoparticle solutions in air.

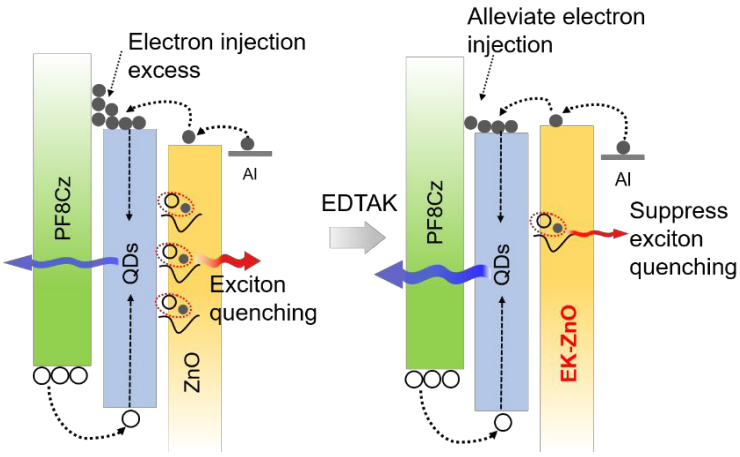

Fig. S12 Schematic of performance enhancement for devices with primordial ZnO and additives-treatment ZnO films.

Table 1. Summary EL Performance of QLEDs with ZnO and EK-ZnO ETLs.

Device	EL (nm)	V_{on} (V)	L_{MAX} (cd/m^2)	CE (cd/A)	PE (lm/W)	EQE (%)
ZnO	468	2.4	14140	6.76	7.08	10.67
EK-ZnO	468	2.4	20060	9.89	9.71	16.31

Table S1 Kinetic parameters obtained from TRPL spectra of Blue QDs deposited on Various substrates.

	τ_1 (ns)	A_1 (%)	τ_2 (ns)	A_2 (%)	τ_{avg} (ns)
Quartz/QDs	0.67	17.17	6.96	82.83	5.88
Quartz/QDs/ZnO	0.67	30.55	5.97	69.45	4.35
Quartz/QDs/EK-ZnO	0.71	23.88	6.52	76.12	5.13

Table S2 Detailed parameters extracted from the UPS and absorption spectra for ZnO and EK-ZnO films.

	Eonset (eV)	Ecutoff (eV)	WF (eV)	VBM (eV)	Eg (eV)	CBM (eV)
ZnO	3.69	17.42	3.80	7.49	3.52	3.97
EK-ZnO	3.65	17.69	3.53	7.18	3.49	3.69

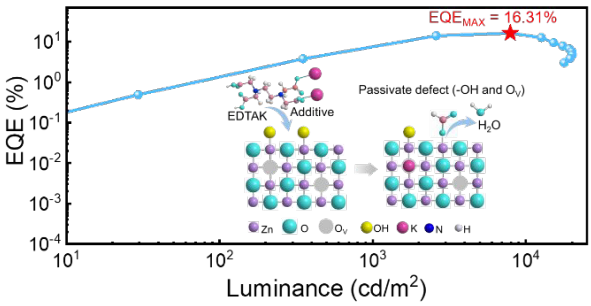

The bifunctional engineering leads to passivate surface defects in ZnO NPs as well as elevating the conduction band level of ZnO to promote charge balance. State-of-the-art blue QLEDs with an EQE of 16.31% and a T_{50}@100 cd/m^2 of 1685 h are achieved.

Supplementary Information

Defect Passivation and Electron Band Energy Regulation of ZnO Electron Transport Layer through a Synergetic Bifunctional Surface Engineering for Efficient Quantum Dot Light-Emitting Diodes

Fensha Cai,[a] Yufei Tu, [b] Dadi Tian, [a] Yan Fang, [a] Bo Hou, [c] Muhammad Ishaq, [d] Xiaohong Jiang, [a] Meng Li, [a] Shujie Wang,[a] Zuliang Du*[a]*

[a] Key Lab for Special Functional Materials of Ministry of Education, National & Local Joint Engineering Research Center for High-efficiency Display and Lighting Technology, School of Materials Science and Engineering, and Collaborative Innovation Center of Nano Functional Materials and Applications,
Henan University,
Kaifeng 475004, China
E-mail: wsj@henu.edu.cn, zld@henu.edu.cn

[b]School of Electronics Information and Intelligent Manufacturing, Sias University, Xinzheng, China

[c]School of Physics and Astronomy, Cardiff University, Cardiff, Wales, CF24 3AA, UK

[d] Institute of Fundamental and Frontier Sciences, University of Electronic Science and Technology of China, Chengdu 610054, China

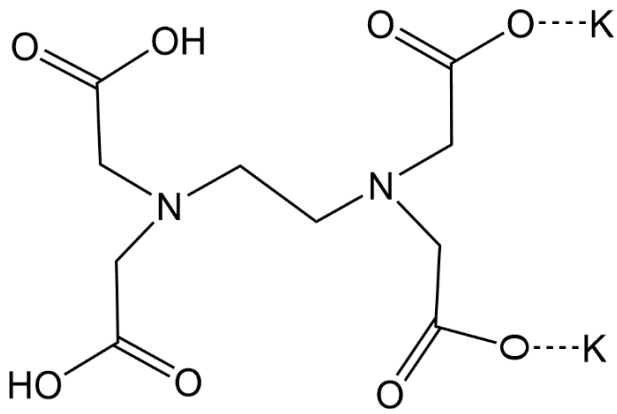

Fig. S1 Molecular structures of EDTAK.

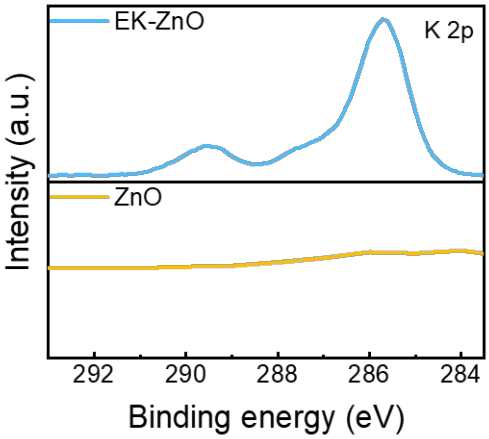

Fig. S2 XPS spectra of K 2p.

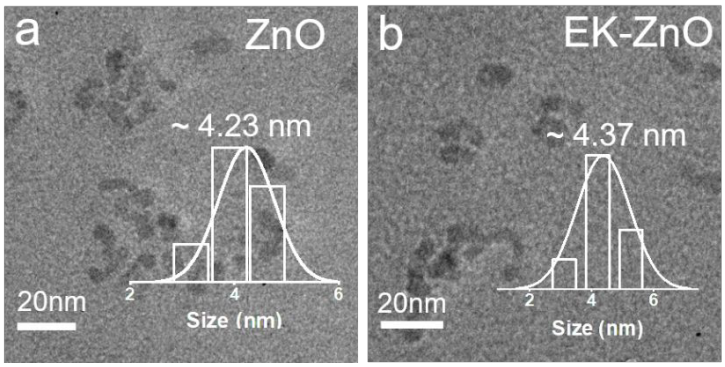

Fig. S3 TEM images of ZnO and EK-ZnO NPs. Insets, corresponding size distribution histogram.

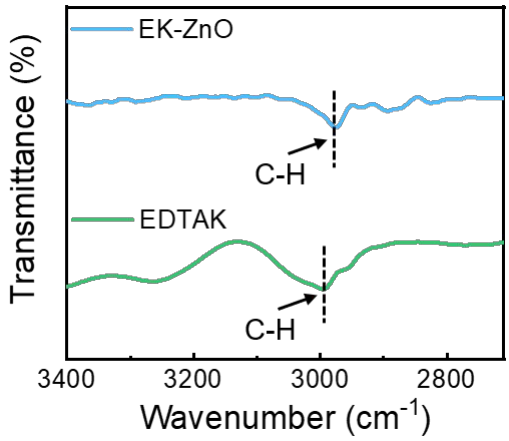

Fig. S4 FTIR of EDTAK and EK-ZnO NPs.

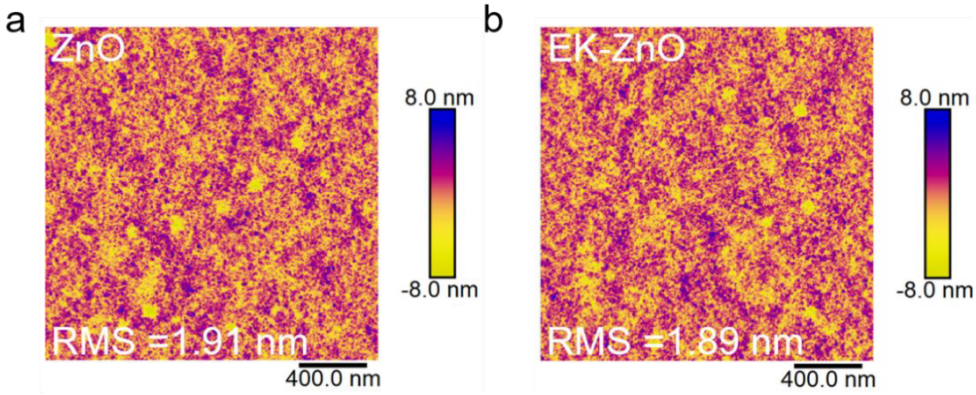

Fig. S5 AFM images of ZnO and EK-ZnO films on glass substrate.

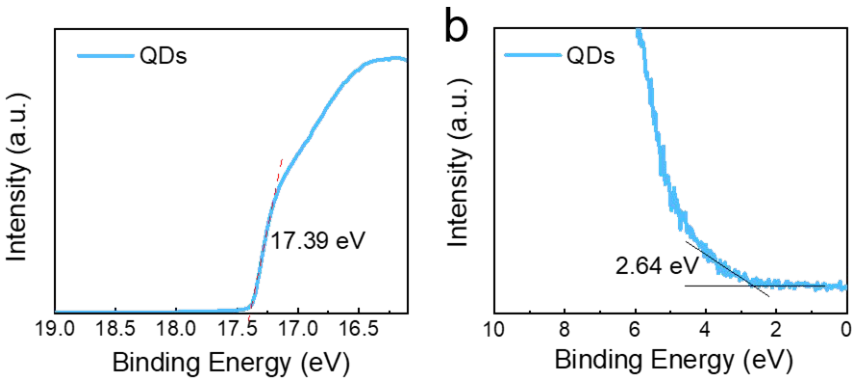

Figure S6. UPS spectra of QDs film on ITO.

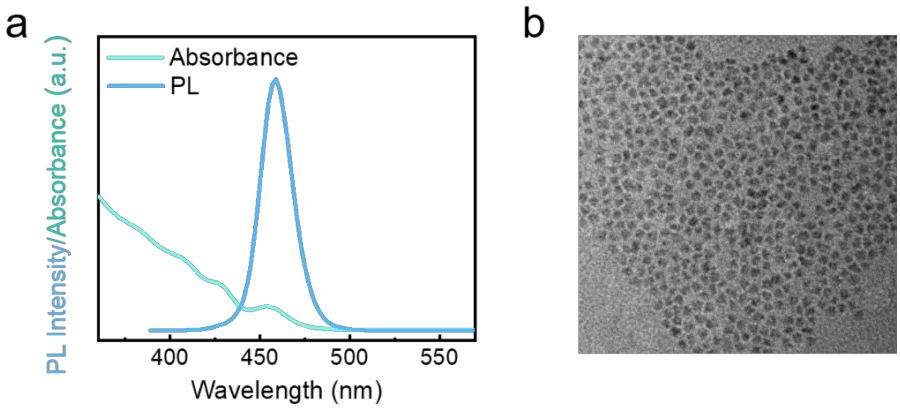

Fig. S7 (a) UV-vis absorption and PL spectra of the CdSe/ZnSe/ZnS QDs. (b) TEM image of CdSe/ZnSe/ZnS QDs.

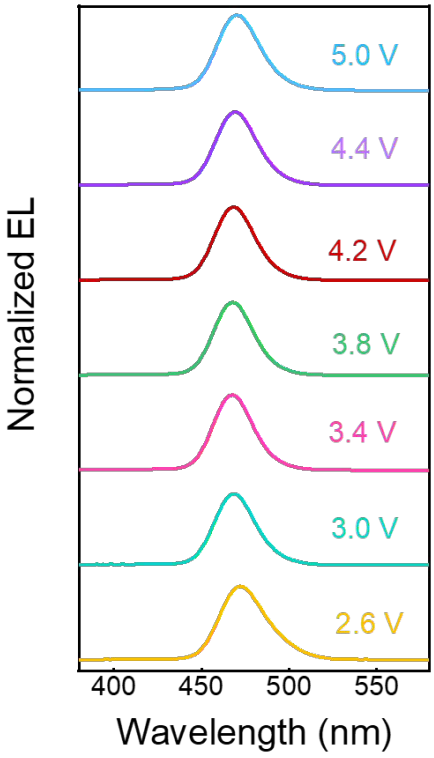

Fig. S8 EL spectra of the QLED with EK-ZnO under an applied voltage of 3.0-5.0 V.

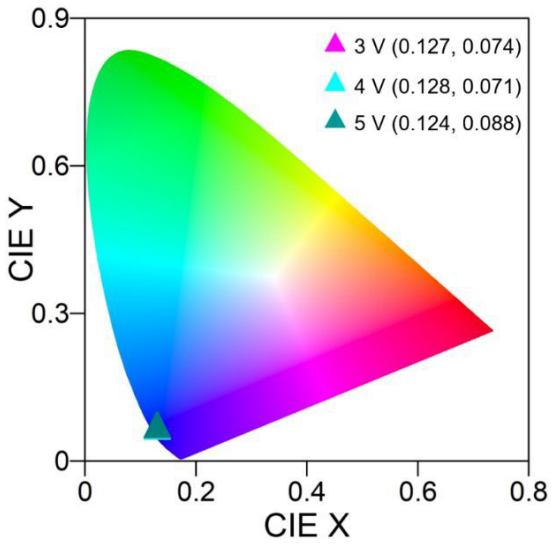

Fig. S9 CIE coordinates of QLEDs based on EK-ZnO ETL under an applied voltage of 3.0-5.0 V.

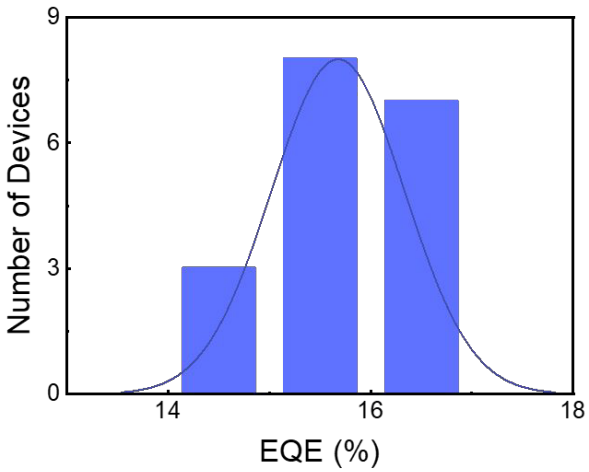

Fig. S10 EQE histogram of 18 devices based on EK-ZnO ETL. The fitting curve is a distribution function curve.

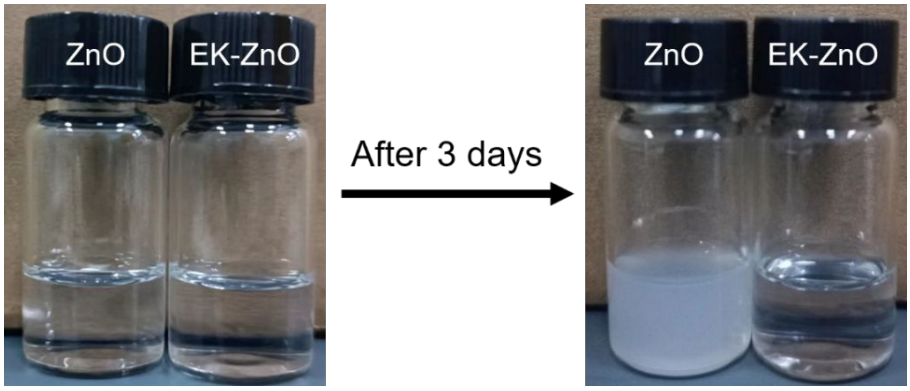

Fig. S11 Photo-graphs of ZnO and EK-ZnO nanoparticle solutions in air.

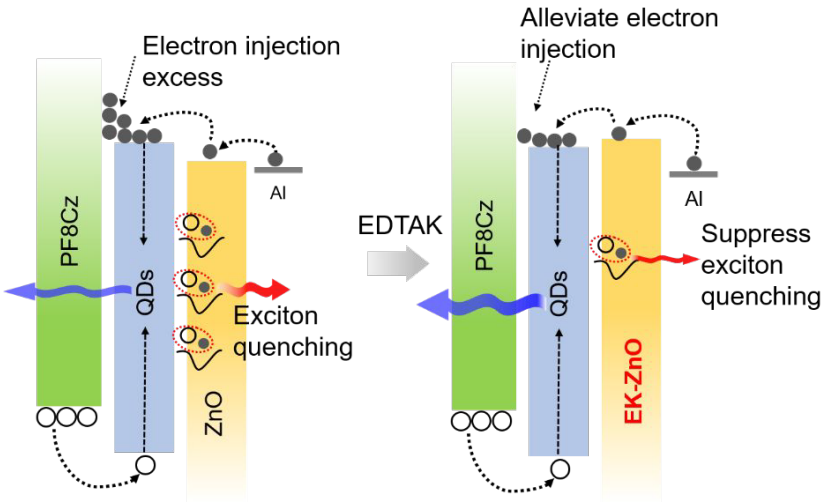

Fig. S12 Schematic of performance enhancement for devices with primordial ZnO and additives-treatment ZnO films.

Table S1 Kinetic parameters obtained from TRPL spectra of Blue QDs deposited on Various substrates.

	τ_1 (ns)	A_1 (%)	τ_2 (ns)	A_2 (%)	τ_{avg} (ns)
Quartz/QDs	0.67	17.17	6.96	82.83	5.88
Quartz/QDs/ZnO	0.67	30.55	5.97	69.45	4.35
Quartz/QDs/EK-ZnO	0.71	23.88	6.52	76.12	5.13

Table S2 Detailed parameters extracted from the UPS and absorption spectra for ZnO and EK-ZnO films.

	Eonset (eV)	Ecutoff (eV)	WF (eV)	VBM (eV)	Eg (eV)	CBM (eV)
ZnO	3.69	17.42	3.80	7.49	3.52	3.97
EK-ZnO	3.65	17.69	3.53	7.18	3.49	3.69